Scalar Wave Diffraction by Tangent Rays

R H Tew* S J Chapman† J R King* J R Ockendon† B J Smith*
I Zafarullah*
** Division of Theoretical Mechanics*
School of Mathematical Sciences
University of Nottingham, Nottingham NG7 2RD, UK
† Mathematical Institute
University of Oxford, 24-29 St Giles', Oxford OX1 3LB, UK

July 6, 2000

Abstract

Modern asymptotic methods are used to provide as complete as possible a description of the scattering of a high-frequency time-harmonic acoustic plane wave by a two-dimensional convex obstacle. The cases of infinite and finite scatterers are considered separately, and descriptions of the diffracted fields and the transition solutions valid across shadow boundaries are presented.

For a finite scatterer, expressions are given for the directivity function (or angular variation) of the scattered field in the very far field encompassing all angular directions; in particular this results in the prediction of a narrow range of angles for which the directivity is an order of magnitude lower than in general.

1 Introduction

Our main intentions in this paper are to present as complete and self-contained an account as possible of the two-dimensional diffraction phenomena that arise as a result of a ray associated with a prescribed short-wavelength acoustic plane wave impinging tangentially on a scattering obstacle, and then to use these results to give a thorough examination of the field that is scattered by a finite, convex obstacle of arbitrary profile (for which there are two such boundary points of ray tangency). This will include descriptions of the wavefields in the 'illuminated' and 'shadow' regions, in the complicated transitions zone between these regions and near to the points of ray tangency themselves. For the case of the finite scatterer, the transition zones adjacent to the two shadow boundaries ultimately merge and this interaction is also described in detail. One interesting feature of this is the construction of the far-field 'directivity' of the scattered field when considered at sufficiently large distances from the scatterer for the latter to appear point-like; in particular, we highlight a very narrow region in which the shadow boundary transitional structure persists for arbitrarily large distances.

Smooth-body diffraction problems such as this have been studied intensively over the last five decades or so, with pioneering analyses presented by Fock [1], Leontovič and Fock [2] and Keller [3]. Propagation into geometrical shadow regions was then incorporated into Keller's celebrated geometrical theory of diffraction [4] via the initiation of a creeping field at points of tangential ray incidence. Reviews of this, and several applications, can be found in [5, 6], whilst a related theory has been developed by Lewis, Bleistein and Ludwig [7].

In addition to the work of Fock and Leontovič [1, 2], early accounts of the excitation problem for creeping waves – the 'inner' problem near points of ray tangency – are given by Zauderer [8, 9].

The literature that exists following these earlier works is immense and it would be impossible to cite all related papers. However, very comprehensive reviews of the Western and Russian literature in the field are given in the books by Bouche et al [10] and by Babič and Buldyrev [11] and Babič and Kirpičnikova [12].

Given this extensive literature, a principal justification of the current paper is that much of the earlier work was performed when powerful asymptotic methods available to us now (and with which we carry out our analysis) were in their infancy, or even non-existent. It is our hope that the systematic solution to this canonical problem in the language of modern asymptotic analysis will provide a springboard for future analytical and computational developments. A good example of recent success of asymptotic analysis is [13] where it is shown that smooth convex scatterers can be conveniently classified into those which are slender, with a radius of curvature at the "tip" being comparable to a wavelength and elsewhere an aspect ratio proportional to the square root of the wavelength, and those which are blunt; the slender case is described in [13] and this paper describes the complementary results for blunt scatterers.

We remark that whilst the full asymptotic solution for the scattered wavefield has been described for certain simple scattering geometries (see Jones [14] and Nussenzveig [15], for example, for the circular and spherical cases, respectively), a self-contained account for an arbitrary convex profile which includes details of the specularly reflected field, all diffraction phenomena and a complete description of the shadow structure at arbitrarily large distances from the obstacle seems to be lacking.

It is also very important to note at this stage new insights into the role played by circular scatterers as paradigms. It was also shown in [13] that diffraction by circular obstacles is *not* generic as far as two-dimensional smooth-body diffraction is concerned. More precisely, it was demonstrated there that the creeping field usually undergoes continuous exponentially small back-reflection as a direct result of the local variation of the boundary curvature with arclength. Thus creeping wave propagation can be likened to one-dimensional propagation through an inhomogeneous medium in which the refractive index is dependent upon position. However, the one circumstance when this does not occur is when the curvature is constant.

Thus, while many existing theories obtain certain diffraction and decay exponents and uniform shadow boundary asymptotics for general obstacles by comparison with the solution for the circular case [6, 10, 16], we believe that it is very important to have a solution which is based on an analysis of an arbitrary profile from the outset without reliance on the solution for a circular (or any other) geometry.

Another new and significant feature worth noting here is that for non-circular, smooth, convex geometries, the classical leading-order modal expansion for the creeping field (such as that described in [6] and discussed at greater length in §2.3 of this paper) exhibits mode-conversion[1], and as such is in need of re-interpretation. The reason for this is that Stokes' phenomenon enables higher modes in this expansion (which are exponentially subdominant to the leading mode) to exhibit apparent discontinuities in their amplitudes across Stokes' surfaces. This mode-conversion implies that all modes other than the first have amplitudes which may depend upon arclength in a piecewise constant fashion and are therefore not constants that can simply be read-off from the analysis of the circular case. This is not the place to go into further details but, as we shall see, the existence of such phenomena has implications for which terms we retain in the asymptotic expansions that follow.

[1]Here, and throughout the rest of this paper, we take 'mode-conversion' to mean the interaction between different terms (or modes) in the creeping field expansion that can take place as a result of Stokes phenomenon.

As with the exponentially small backward-propagating creeping field, which can also be explained in terms of such mode-conversion, this phenomenon can be analysed using optimal truncation [17] and does not arise in the circular (i.e. constant curvature) situation. The systematic application of matched asymptotic expansions identifies what can be regarded as true canonical problems, the Fock-Leontovič inner problem of section 2.2 being the key one in the current context.

We now proceed by beginning with the ray tangency problem for the simplest case of an infinite convex body. We will then use these results to treat the diffraction of a plane wave by an arbitrary finite, convex obstacle.

We present the results for the Dirichlet (i.e. 'soft') boundary condition in the main text; the analogous formulae for the Neumann ('hard') case are listed in the Appendix.

2 Infinite Scatterers

2.1 Governing equations and the specularly reflected field

We begin by defining the geometry of the scatterer, the nature of the incident field and the governing equations for the diffraction problem we are studying.

We suppose that the incoming plane wave is given by a potential $\phi_i(x,t) = e^{ikx-i\omega t}$ where the wavenumber k and temporal frequency ω are related by $\omega/k = c$, where c is the propagation speed. Henceforth, the factor $e^{-i\omega t}$ is implied but omitted. This wave propagates in the semi-infinite region $D \subset \mathbb{R}^2$ adjacent to the open, convex body ∂D parametrised by arclength s in the form $x = x_0(s)$, $y = y_0(s)$ or, in vector notation, $\boldsymbol{x} = \boldsymbol{x}_0(s)$ (see Fig. 1). As we shall see, it is convenient to have x and s increasing in the same sense and so we adopt the convention that arclength increases in a clockwise direction. If this is so, then we can define a local unit tangent vector $\boldsymbol{t}(s)$, a local unit normal vector $\boldsymbol{n}(s)$ and a (positive) boundary curvature $\kappa(s)$ which satisfy the two-dimensional Serret-Frenet relations

$$\frac{d\boldsymbol{x}_0}{ds} = \boldsymbol{t}, \quad \frac{d\boldsymbol{n}}{ds} = \kappa\boldsymbol{t}, \quad \frac{d\boldsymbol{t}}{ds} = -\kappa\boldsymbol{n}. \tag{2.1}$$

The full boundary value problem to be solved for the total potential ϕ is the Helmholtz equation

$$\frac{1}{(1+n\kappa)}\frac{\partial}{\partial n}\left[(1+n\kappa)\frac{\partial\phi}{\partial n}\right] + \frac{1}{(1+n\kappa)}\frac{\partial}{\partial s}\left[\frac{1}{(1+n\kappa)}\frac{\partial\phi}{\partial s}\right] + k^2\phi = 0, \quad n > 0, \tag{2.2}$$

in a region sufficiently close to the scatterer for n, the normal distance from ∂D into D, to be defined. We impose a Dirichlet boundary condition

$$\phi = 0 \quad \text{on} \quad \partial D \tag{2.3}$$

(results corresponding to the Neumann condition $\partial\phi/\partial n = 0$ are listed in the Appendix) and the far-field condition that $\phi - e^{ikx}$ must be outgoing.

In the short-wavelength limit $k \to \infty$, we first pose a ray ansatz for the specularly reflected field ϕ_r in the form

$$\phi_r(x,y) \sim \sum_{n=0}^{\infty} \frac{A_n(x,y)}{(ik)^n} e^{iku(x,y)} \tag{2.4}$$

from which the eikonal equation

$$\boldsymbol{\nabla} u \cdot \boldsymbol{\nabla} u = 1 \tag{2.5}$$

and the recursive system of transport equations

$$
\begin{aligned}
A_0 \nabla^2 u + 2\boldsymbol{\nabla} A_0 \cdot \boldsymbol{\nabla} u &= 0 && \text{(2.6a)}\\
A_n \nabla^2 u + 2\boldsymbol{\nabla} A_n \cdot \boldsymbol{\nabla} u &= -\nabla^2 A_{n-1} \quad (n = 1, 2, 3) && \text{(2.6b)}
\end{aligned}
$$

follow by substitution into the Helmoltz equation and balancing equal powers of k^{-1}.

The rays are the characteristics of (2.5) and if τ is distance along a ray, with $\tau = 0$ on ∂D, then we see that the equations of the rays satisfy

$$\frac{d\boldsymbol{x}}{d\tau}(\tau, s) = \boldsymbol{\nabla} u(0, s), \quad \boldsymbol{x}(0, s) = \boldsymbol{x}_0(s) \tag{2.7}$$

along which (2.5) has the solution $u = u_0(s) + \tau$, where $u_0(s)$ is the boundary value of u, and the transport equations (2.6a, 2.6b) reduce to ordinary differential equations. The leading order transport equation (2.6a) can then be integrated explicitly to give

$$A_0(\tau, s) = A_0(0, s)\left[\frac{q_0(s)x_0'(s) - p_0(s)y_0'(s)}{\tau\left(q_0(s)p_0'(s) - p_0(s)q_0'(s)\right) + q_0(s)x_0'(s) - p_0(s)y_0'(s)}\right]^{\frac{1}{2}} \tag{2.8}$$

where $\boldsymbol{\nabla} u(0, s) = (p_0(s), q_0(s))$. In this case, the specified phase and amplitude of the incident field imply that $u_0(s) = x_0(s)$ and $A_0(0, s) = -1$ ($+1$ for Neumann data); we then find that leading-order reflected field is given by

$$\phi_r \sim -\left[\frac{\sin\psi(s)}{2\kappa(s)\tau + \sin\psi(s)}\right]^{\frac{1}{2}} e^{ik(x_0(s)+\tau)} \tag{2.9}$$

where the angle of curvature $\psi(s)$ is defined by $\boldsymbol{t}(s) = (\cos\psi(s),\ \sin\psi(s))$, in terms of which the ray equations are $\boldsymbol{x} = \boldsymbol{x}_0(s) + \tau\left(\cos\left(2\psi(s)\right), \sin\left(2\psi(s)\right)\right)$.

This expression is valid for reflection at all points on the boundary $\tau = 0$ for which $\psi(s) \neq 0$ (i.e. at points of specular reflection), ϕ_r being indeterminate on ∂D when $\sin\psi(s) = 0$ (since then $\tau = 0$ and $\sin\psi(s) = 0$ simultaneously). Hence, (2.9) is not valid at boundary points for which the tangent to ∂D is parallel to the x-axis, which is precisely the condition for one of the incoming rays to impinge upon the boundary tangentially.

The problem must be re-examined in the vicinity of this point, and this will be done in the next sub-section.

2.2 Diffraction analysis near the point of ray tangency

Near the boundary point of ray tangency, we must abandon the ray solution (2.9) and seek an inner solution based on another suitable approximation to the Helmholtz equation (2.2). To do this, we choose a local coordinate system with the origin at the point of tangency and the y-axis directed along the outward normal to ∂D. We also take s to be measured from this point.

If we write the total potential in the form

$$\phi = e^{ikx} + e^{iks}A(s, n), \tag{2.10}$$

then the appropriate local scalings on s and n are

$$s = k^{-\frac{1}{3}}\kappa_0^{-\frac{2}{3}}\hat{s}, \quad n = k^{-\frac{2}{3}}\kappa_0^{-\frac{1}{3}}\hat{n} \tag{2.11}$$

where κ_0 is the curvature of the boundary at the point of tangency. We assume here that κ_0 is non-zero and that $\kappa_0 \ll k$. The case $\kappa_0 = 0$ corresponds to a boundary that is not locally parabolic, and leads to a difficult diffraction problem, whilst $\kappa_0 = O(k)$ corresponds to a body with a sharp tip that is in the parameter regime defining the transition between the slender "Sommerfeld" and blunt "Fock-Leontovič" diffraction regimes [13].

The leading-order inner amplitude $\hat{A}(\hat{s},\hat{n})$ satisfies the well-known Fock-Leontovič equation [2]

$$\frac{\partial^2 \hat{A}}{\partial \hat{n}^2} + 2i\frac{\partial \hat{A}}{\partial \hat{s}} + 2\hat{n}\hat{A} = 0, \quad \hat{n} > 0 \ , \tag{2.12}$$

and with Dirichlet data, $\hat{A}$ satisfies the boundary condition

$$\hat{A}(\hat{s},\ 0) = -e^{-i\hat{s}^3/6} \ , \tag{2.13}$$

the derivation of which requires the fact that locally x and y are given by

$$x \sim s + k^{-1}\left(\hat{n}\hat{s} - \tfrac{1}{6}\hat{s}^3\right),\ y \sim k^{-2/3}\kappa_0^{-1/3}(\hat{n} - \tfrac{1}{2}\hat{s}^2). \tag{2.14}$$

In addition to this, having explicitly subtracted out the incident field in (2.10) we must impose an outgoing-wave condition on the scattered field.

The solution for $\hat{A}(\hat{s},\hat{n})$ which satisfies all of these conditions can be obtained by taking a Fourier transform in $\hat{s}$ and the expression

$$\hat{A}(\hat{s},\ \hat{n}) = -2^{\frac{1}{3}}\int_{-\infty}^{\infty}\frac{\mathrm{Ai}(-2^{\frac{1}{3}}p)Ai\left(-2^{\frac{1}{3}}\,(p+\hat{n})\,e^{2\pi i/3}\right)e^{-i\hat{s}p}}{Ai\left(-2^{\frac{1}{3}}e^{2\pi i/3}p\right)}dp \tag{2.15}$$

results, where $Ai(\cdot)$ is the Airy function.

We will repeatedly use this solution when matching with the outer solutions to be derived in the following sections; this procedure is sometimes best implemented in local cartesian coordinates rather than $\hat{s}$ and $\hat{n}$ and to facilitate this, we could re-express (2.10) in the form

$$\phi \quad = \quad e^{ikx}\left(1 + B\left(x,y\right)\right) \tag{2.16}$$

and scale

$$x \quad = \quad k^{-\frac{1}{3}}\kappa_0^{-\frac{2}{3}}\hat{x}, \quad y = k^{-\frac{2}{3}}\kappa_0^{-\frac{1}{3}}\hat{y}. \tag{2.17}$$

In this case, the local form of ∂D is $\hat{y} + \frac{1}{2}\hat{x}^2 = 0$, noting that if ∂D is expressed as $y = f(x)$, then $f(0) = f'(0) = 0$ and $\kappa_0 = -f''(0)$. The boundary value problem to be solved for the inner form of the scattered amplitude $\hat{B}(\hat{x},\hat{y})$ is then

$$\frac{\partial^2 \hat{B}}{\partial \hat{y}^2} + 2i\frac{\partial \hat{B}}{\partial \hat{x}} = 0, \quad \hat{y} + \tfrac{1}{2}\hat{x}^2 > 0, \tag{2.18}$$

$$\hat{B} = -1, \quad \hat{y} + \tfrac{1}{2}\hat{x}^2 = 0. \tag{2.19}$$

Hence, in this formulation we see that the field equation has been simplified – it now has constant coefficients – but the boundary conditions are now specified on a curve. To relate to (2.12), we follow Fock's procedure [1] (Ch.5) and introduce new coordinates

$$\hat{\zeta} = \hat{y} + \tfrac{1}{2}\hat{x}^2, \quad \hat{\xi} = \hat{x} \tag{2.20}$$

and a new dependent variable $\hat{w}(\hat{\zeta},\hat{\xi})$ defined by

$$\hat{B}(\hat{x},\hat{y}) = e^{-i\hat{\zeta}\hat{\xi}+i\hat{\xi}^3/6}\hat{w}(\hat{\zeta},\hat{\xi}). \tag{2.21}$$

Then the problem to be solved for $\hat{w}$ is

$$\frac{\partial^2 \hat{w}}{\partial \hat{\zeta}^2} + 2i\frac{\partial \hat{w}}{\partial \hat{\xi}} + 2\hat{\zeta}\hat{w} = 0, \quad \hat{\zeta} > 0, \tag{2.22}$$

$$\hat{w} = -e^{-i\hat{\xi}^3/6}, \quad \hat{\zeta} = 0, \tag{2.23}$$

which is identical in form to the Fock-Leontovič equation (2.12) and we can therefore use the solution (2.15), together with the preceding string of coordinate transformations, to obtain a closed-form expression for $\hat{B}(\hat{x}, \hat{y})$. This is of no real surprise since a straightforward calculation shows that to leading order, $\hat{\xi} = \hat{s}$, $\hat{\zeta} = \hat{n}$ and that the exponential prefactor in (2.21) is precisely that required to convert the e^{ikx} factor multiplying B in (2.16) into the e^{iks} factor that led to (2.12) (so that $\hat{w}$ and $\hat{A}$ are also equal to leading order).

The results of this section provide the solution close to the point of tangency for a wide class of convex scatterers and we will see that they apply whether they are finite or infinite. We now use this information to determine the asymptotic solution for the wavefield elsewhere.

2.3 Near-surface wave structure in deep shadow

To construct the solution for ϕ in the shadow zone well removed from the Fock-Leontovič region discussed in §2.2 but near the boundary, we must replace the scalings (2.11) by

$$s = O(1), \quad n = k^{-\frac{2}{3}}\bar{n}, \tag{2.24}$$

where we note that we have not introduced an explicit dependence upon local curvature in the scaling on n. It turns out that when this scaling is inserted into the Helmholtz equation, an appropriate ansatz to take for the *total* potential ϕ is

$$\phi(s, \bar{n}) \sim e^{iks + ik^{\frac{1}{3}} f(s,\bar{n})} \sum_{M=0}^{\infty} \frac{C_M(s, \bar{n})}{k^{M/3}}, \tag{2.25}$$

though we note that in order to be consistent with the leading-order approach developed so far we only calculate the leading-order term here (i.e., that involving C_0).

The leading-order equation arising from substituting (2.25) into (2.2) is

$$\left(\frac{\partial f}{\partial \bar{n}}\right)^2 = 0, \tag{2.26}$$

so that $f = f(s)$. The next term yields the Airy equation

$$\frac{\partial^2 C_0}{\partial \bar{n}^2} + 2\left(\bar{n}\kappa(s) - f'(s)\right) C_0 = 0 \tag{2.27}$$

for C_0, in which the function $f'(s)$ appears as an eigenvalue. Imposing the radiation condition on C_0, the solution is

$$C_0(s, \bar{n}) = \gamma(s) Ai\left(-2^{\frac{1}{3}}\kappa^{\frac{1}{3}}(s)\left(\bar{n} - f'(s)/\kappa(s)\right) e^{2\pi i/3}\right) \tag{2.28}$$

where $\gamma(s)$ is yet to be determined. Use of the boundary condition now gives that

$$f'(s) = \frac{-\lambda_m^2 \kappa^{\frac{2}{3}}(s) e^{-2\pi i/3}}{2^{\frac{1}{3}}}, \qquad \mathrm{Ai}\left(-\lambda_m^2\right) = 0 \quad (\text{with } \lambda_0 < \lambda_1 < \lambda_2 \ldots). \tag{2.29}$$

We obtain the equation for C_1 by considering the next term arising from the Helmholtz equation and this turns out to be

$$\frac{\partial^2 C_1}{\partial \bar{n}^2} + 2\left(\bar{n}\kappa(s) - f'(s)\right) C_1 + 2i\frac{\partial C_0}{\partial s} = 0 \tag{2.30}$$

where $f'(s)$ is now given by (2.29).

This equation can be used together with (2.27) to show that the solvability condition for either Neumann or Dirichlet data is

$$\frac{d}{ds}\int_0^\infty C_0^2(s,\bar{n})d\bar{n} = 0, \tag{2.31}$$

from which it follows that the amplitude coefficient $\gamma(s)$ satisfies the ordinary differential equation

$$\frac{1}{\gamma}\frac{d\gamma}{ds} = \frac{1}{6\kappa}\frac{d\kappa}{ds}, \tag{2.32}$$

so that

$$\gamma(s) = \alpha\left(\kappa(s)\right)^{\frac{1}{6}}, \tag{2.33}$$

where α is an as yet unknown constant. As with the derivation of (2.31), this general solution for $\gamma(s)$ is valid for both Dirichlet and Neumann data, though the value of the constant α does depend upon whether the scatterer is hard or soft.

It now follows from (2.28) and (2.29) that (2.25) can formally be generalised to a sum of modes in the form

$$\phi(s,\bar{n}) \sim e^{iks}\sum_{m=0}^{\infty} e^{ik^{1/3}f_m(s)}\sum_{M=0}^{\infty}\frac{C_{Mm}(s,\bar{n})}{k^{M/3}}, \tag{2.34}$$

where we have made explicit the dependence of the amplitude functions C_{Mm} and the phase function f_m upon the mode number m. In this expression a fixed value of M, which corresponds to a single term in the original expansion (2.25), is now itself an infinite series. Though we must take great care in interpreting this modal expansion (see the comments to follow), the C_{0m} terms can loosely be understood to be the leading-order (in k) modes and which match with all the terms in the large $\tilde{s}$ expansion of the zeroth-order Fock-Leontovič solution derived in §2.2; we will shortly implement this matching explicitly to loeading order. Higher order Fock-Leontovič solutions (not considered in this paper) would be associated with the C_{im} $(i > 1)$ amplitude terms.

The asymptotic nature of the solution we are deriving here needs very careful interpretation. This is because the fact that $Im(f_{m+1}) > Im(f_m) > 0,\ m = 0, 1, \ldots,$ implies an exponential decay of the solution with s, with each mode being exponentially subdominant to the previous one. Thus the first mode has an algebraic series ($m = 0$, sum over M) which is exponentially dominant over all subsequent modes and, moreover, is in general divergent. Since our solution has only been derived to leading-order in powers of k, there is no justification for retaining these higher-order modes and we are forced to restrict attention to the first mode and we retain the $m = 0$, $M = 0$ term in (2.34) only, so that

$$\phi(s,\bar{n}) \sim e^{iks}e^{ik^{1/3}f_0(s)}C_{00}(s,\bar{n}). \tag{2.35}$$

We are now able to piece together the results that we have obtained so far to yield

$$\begin{aligned}&\phi(s,\bar{n}) \sim \alpha_0 \kappa^{\frac{1}{6}}(s) e^{iks} \mathrm{Ai}\left(-2^{\frac{1}{3}}\kappa^{\frac{1}{3}}(s)\left(\bar{n}+\frac{\lambda_0^2 e^{-2\pi i/3}}{\kappa^{1/3}(s)2^{1/3}}\right)e^{2\pi i/3}\right)\times \\ &\exp\left(ik^{\frac{1}{3}}\left(\frac{-\lambda_0^2 e^{-2\pi i/3}}{2^{1/3}}\int_0^s \kappa^{\frac{2}{3}}(t)dt+\beta_0\right)\right)\end{aligned} \tag{2.36}$$

where β_0 is the constant of integration in the determination of $f(s)$ from (2.29), with $m = 0$.

The unknown constants α_0 and β_0 are determined by matching the outer solution (2.36) with the inner solution (2.15). In fact, this is straightforward to do since what is required is the sum of residues $\hat{A}_R(\hat{s},\hat{n})$ associated with (2.15), this being

$$\hat{A}_R(\hat{s},\hat{n}) = -2\pi i e^{-2\pi i/3}\sum_{m=0}^{\infty}\frac{\mathrm{Ai}\left(-\lambda_m^2 e^{-2\pi i/3}\right)\mathrm{Ai}\left(-\lambda_m^2-2^{\frac{1}{3}}e^{2\pi i/3}\hat{n}\right)\exp\left(-i2^{-\frac{1}{3}}e^{-2\pi i/3}\lambda_m^2\hat{s}\right)}{\mathrm{Ai}'(-\lambda_m^2)}, \tag{2.37}$$

in terms of the inner coordinates $\hat{s}$ and $\hat{n}$ introduced in §2.1. As $\hat{s}\to\infty$, the first term dominates and this matches (2.36) provided

$$\alpha_0 = -\frac{2\pi i \mathrm{Ai}(-\lambda_0^2 e^{-2\pi i/3})e^{-2\pi i/3}}{\kappa_0^{1/6}\mathrm{Ai}'(-\lambda_0^2)}, \quad \beta_0 = 0. \tag{2.38}$$

We have now constructed the solution close to the boundary, both near the point of ray tangency and away from it in the shadow region. It is this region that gives birth to the diffracted creeping ray field that is shed into the shadow region and we now systematically derive the asymptotic structure of the field in the shadow zone moving from the scattering surface towards and through the shadow boundary, finally ending in the illuminated region.

2.4 The shed creeping field

To determine the wave structure outside the "Airy-layer" solution (2.36), we seek a leading-order solution in the form

$$\phi \sim k^{\nu} D_0 e^{iku+ik^{\frac{1}{3}}v}, \tag{2.39}$$

this being motivated by the expansion (2.25). We must now determine the functions D_0, u and v, all of which are independent of k, and the exponent ν.

Substitution of (2.39) into the Helmholtz equation, this time for $O(1)$ values of both s and n, and balancing equal powers of k gives

$$(\boldsymbol{\nabla} u)\cdot(\boldsymbol{\nabla} u) = 1, \tag{2.40}$$

$$(\boldsymbol{\nabla} u)\cdot(\boldsymbol{\nabla} v) = 0 \tag{2.41}$$

and

$$2(\boldsymbol{\nabla} D_0)\cdot(\boldsymbol{\nabla} u) + D_0\nabla^2 u = 0. \tag{2.42}$$

Since (2.39) must match into (2.36) as the boundary is approached, appropriate boundary data $u = u_0(s)$ for the eikonal equation (2.40) is given in terms of arclength s by

$$u_0(s) = s\ . \tag{2.43}$$

From this, it follows that the rays of the eikonal equation leave the boundary tangentially, so the boundary is a caustic of the ray field associated with (2.39). The solution local to a caustic is well known to be described by Airy functions [18] and this is consistent with the Airy layer solution (2.36).

If we now introduce ray coordinates (ρ, τ), where ρ is arclength along the boundary to the point of departure of the ray and τ is the distance along the shed ray, it follows from (2.40) and (2.43) that in terms of these coordinates

$$u(\rho, \tau) = \rho + \tau \ . \tag{2.44}$$

Since the rays propagate in the direction of $\boldsymbol{\nabla} u$, (2.41) shows that v has no variation with τ so that $v = v(\rho)$. Also, given the solution (2.44), (2.42) can be solved to obtain

$$D_0(\rho, \tau) = \frac{F(\rho)}{\tau^{1/2}} \tag{2.45}$$

for some function F.

Again, noting that the solution that we derive here must match into (2.36), we are led to combine the results obtained so far and write the leading-order solution in the form

$$\phi \sim \frac{k^{\nu} F(\rho) e^{ik(\rho+\tau)+ik^{\frac{1}{3}}v(\rho)}}{\tau^{1/2}} \ . \tag{2.46}$$

The exponent ν and the unknown functions F and v are obtained by this matching condition, and they turn out to be $\nu = -\frac{1}{6}$,

$$F(\rho) = -\frac{\pi^{1/2} e^{-i\pi/12} 2^{1/6} \mathrm{Ai}(-\lambda_0^2 e^{-2\pi i/3})}{\kappa_0^{1/6} \kappa^{1/6}(\rho) \mathrm{Ai}'(-\lambda_0^2)} \tag{2.47}$$

and

$$v(\rho) = -\lambda_0^2 e^{-2\pi i/3} 2^{-\frac{1}{3}} \int_0^{\rho} \kappa^{\frac{2}{3}}(t) dt \ . \tag{2.48}$$

When performing this matching calculation, we need to recall the relation between the coordinates (s, n) and the ray co-ordinates (ρ, τ). The position vector of a general point exterior to the boundary can be expressed in the two equivalent forms $\boldsymbol{x}_0(\rho) + \tau \boldsymbol{t}(\rho)$, where $\boldsymbol{t}(\rho)$ is the tangent at the point whose arclength is ρ, and $\boldsymbol{x}_0(s) + n\boldsymbol{n}(s)$, where $\boldsymbol{n}$ is the local unit normal at the point at arclength s. Equating these two expressions and imposing the relevant scalings allows one co-ordinate system to be converted into the other. For example, if we scale $\tau = k^{-\frac{1}{3}}\bar{\tau}$ ($\bar{\tau} = O(1)$) and consider $O(1)$ values of ρ, then

$$s \sim \rho + k^{-\frac{1}{3}}\bar{\tau} - \tfrac{1}{3}k^{-1}\kappa^2(\rho)\bar{\tau}^3$$

and

$$n \sim \tfrac{1}{2}k^{-\frac{2}{3}}\kappa(\rho)\bar{\tau}^2 + \tfrac{1}{6}k^{-1}\kappa'(\rho)\bar{\tau}^3$$

follow.

The ray structure emerging into the shadow region from the Airy layer that hugs the boundary has thus been identified as being shed tangentially from a creeping surface ray propagating around the back of the body. These shed rays, which having left the boundary are real, propagating rays (with no exponential decay in τ), get weaker in amplitude as the corresponding point of emission moves deeper into the shadow zone, because the factor $e^{ik^{\frac{1}{3}}v(\rho)}$ present in (2.46) implies that each mode decays exponentially with ρ.

2.5 Shadow boundary structure

The next region to consider is the transition from the shadow region into the "illuminated" region. We will see that this calculation exposes a three-layer asymptotic wave structure in this transition zone and we motivate it by first posing the traditional shadow boundary scalings

$$x = O(1), \quad y = k^{-1/2}\hat{y} \tag{2.49}$$

and seek a solution for the total potential in the form

$$\phi(x,\hat{y}) \sim e^{ikx}A_{SB}(x,\hat{y}) \ . \tag{2.50}$$

We then see that the leading-order amplitude A satisfies

$$\frac{\partial^2 A_{SB}}{\partial \hat{y}^2} + 2i\frac{\partial A_{SB}}{\partial x} = 0, \qquad x > 0, \tag{2.51}$$

where, to match with the solution in the Fock-Leontovič region, we require

$$A_{SB}(0,\hat{y}) = H(\hat{y}), \tag{2.52}$$

where $H(\cdot)$ is the Heaviside function. The solution to this problem is

$$A_{SB}(x,\hat{y}) = \tfrac{1}{2}\mathrm{erfc}\left(-\frac{e^{-i\pi/4}\hat{y}}{\sqrt{(2x)}}\right), \tag{2.53}$$

which can also be written in terms of the Fresnel integral $F(z) = \int\limits_z^\infty e^{iw^2}dw$ in the form

$$A_{SB}(x,\hat{y}) = \frac{e^{-i\pi/4}}{\sqrt{\pi}}F\left(-\frac{\hat{y}}{\sqrt{(2x)}}\right). \tag{2.54}$$

However, we know that this cannot represent the full transitional solution since it can be shown that (2.53) does not match into the diffracted field that was derived in the previous section; nor for that matter does it match into the specularly reflected field as we pass right through the shadow boundary into the illuminated region.

We therefore need to construct intermediate asymptotic layers adjacent to the upper and lower edges of the traditional shadow boundary in order to achieve this matching. To motivate the appropriate scalings, we note that the limiting reflected rays neighbouring the Fock-Leontovič zone and the 'upper' shadow boundary (i.e. that bordering the illuminated region) come from points for which $s = -k^{-\frac{1}{3}}\bar{s}$, where $\bar{s}$ is $O(1)$ and positive. From the ray equations in the paragraph following (2.9), this implies that $y = O(k^{-\frac{1}{3}})$ along these rays at $O(1)$ distances along them and so in the current calculation we now scale

$$x = O(1), \quad y = k^{-\frac{1}{3}}\tilde{y} \ . \tag{2.55}$$

In this case, if we write $\tilde{\phi}(x,\tilde{y}) \sim k^{\mu}e^{ikx}\tilde{A}_{SB}(x,\tilde{y})$ (where μ is to be determined along with $\tilde{A}_{SB}$) then $\tilde{A}_{SB}$ satisfies the equation

$$\frac{\partial^2 \tilde{A}_{SB}}{\partial \tilde{y}^2} + 2ik^{\frac{1}{3}}\frac{\partial \tilde{A}_{SB}}{\partial x} + k^{-\frac{2}{3}}\frac{\partial^2 \tilde{A}_{SB}}{\partial x^2} = 0. \tag{2.56}$$

This motivates the leading-order ansatz

$$\tilde{A}_{SB}(x,\tilde{y}) \sim \tilde{A}_0(x,\tilde{y})e^{ik^{\frac{1}{3}}\tilde{u}(x,\tilde{y})} \tag{2.57}$$

from which it follows that

$$\left(\frac{\partial \tilde{u}}{\partial \tilde{y}}\right)^2 + 2\frac{\partial \tilde{u}}{\partial x} = 0 \tag{2.58}$$

and

$$2\frac{\partial \tilde{u}}{\partial \tilde{y}}\frac{\partial \tilde{A}_0}{\partial \tilde{y}} + 2\frac{\partial \tilde{A}_0}{\partial x} + \tilde{A}_0\frac{\partial^2 \tilde{u}}{\partial \tilde{y}^2} = 0. \tag{2.59}$$

Notice that the trivial solution $\tilde{u}(x,\tilde{y}) \equiv 1, \tilde{A}_0(x,\tilde{y}) \equiv 1$ and the choice $\mu = 0$ reproduce the incident field and this will be a part of the solution valid in $\tilde{y} > 0$, but not in $\tilde{y} < 0$ where there is no incident field. We will shortly see that the complete determination of $\tilde{A}_0$ involves matching into the appropriate limit of the Fock-Leontovič solution (2.15); the latter calculation takes different forms depending upon whether or not we are in the illuminated region and this automatically accounts for the incident field to which we have just referred.

A straightforward analysis by the method of characteristics gives us the relevant solutions to (2.58) of the form

$$\tilde{u}(x,\tilde{y}) = \frac{\tilde{y}^2}{2x} + \tilde{u}_0, \tag{2.60}$$

where $\tilde{u}_0$ is a constant, and then (2.59) reduces to

$$2\left(x\frac{\partial \tilde{A}_0}{\partial x} + \tilde{y}\frac{\partial \tilde{A}_0}{\partial \tilde{y}}\right) + \tilde{A}_0 = 0. \tag{2.61}$$

The general solution to (2.61) is

$$\tilde{A}_0(x,\tilde{y}) = x^{-\frac{1}{2}}g\left(\tilde{y}/x\right) \tag{2.62}$$

for an as yet unknown function g of the single variable $\tilde{y}/x$.

We must find this function g (which we will later find to be crucial in describing the far-field 'directivity') and the constants μ and $\tilde{u}_0$ by matching (2.15) into the Fock-Leontovič solution (2.16) and, after some involved calculations, the result is that $\mu = -\frac{1}{6},\ \tilde{u}_0 = 0$ and

$$g(\xi) = -(2\pi)^{-1/2}\kappa_0^{-\frac{1}{3}}e^{i\pi/12}e^{-i\xi^3/6\kappa_0}\int_{-\infty}^{\infty}\frac{\mathrm{Ai}(-2^{\frac{1}{3}}p)}{\mathrm{Ai}(-2^{\frac{1}{3}}e^{2\pi i/3}p)}e^{ip\xi/\kappa_0^{\frac{1}{3}}}\,dp\ . \tag{2.63}$$

This single expression is valid for both upper and lower transition zones (remember, though, that the incident field must be added to this transitional solution in $\tilde{y} > 0$) and another involved calculation confirms that this solution successfully matches into the error function profile (2.53) from either direction. It can also be shown that there is a successful match between the lower transition zone and the creeping field and between the upper transition zone and the appropriate limit of the specularly reflected ray field, though details of this somewhat tedious and involved calculation are also omitted here.

This transition solution derived from the initial ansatz (2.57) can be thought of as being a "ray limit" shadow boundary solution.

2.6 Matching between the Fock-Leontovič region and the reflected field

We have now constructed a complete asymptotic picture of the field in the shadow region, deriving solutions valid away from the point of tangency and incorporating all regions from the boundary into the illuminated zone. One calculation that remains is to check that we have a smooth match between the Fock-Leontovič solution and the 'geometrical optics' solution. This is achieved by stationary phase estimates of (2.15) for $\hat{s}$ and $\hat{n}$ large with $\hat{s}/\sqrt{\hat{n}} = O(1)$. This calculation shows that there are different estimates according as $\hat{s}^2/2\hat{n} > 1$ or $\hat{s}^2/2\hat{n} < 1$, which is no real surprise since $\hat{s}^2/2\hat{n} = 1$ is the inner equation of the geometrical shadow boundary.

If $\hat{s}^2/2\hat{n} > 1$ then we are examining the solution in shadow and the stationary phase estimate of (2.15) is $-e^{i\hat{n}\hat{s}-i\hat{s}^3/6}$, exactly cancelling the incident field (as expected). Conversely, if $\hat{s}^2/2\hat{n} < 1$ there is a contribution of amplitude

$$\frac{-\sqrt{2}\,(1-\hat{s}^2/2\hat{n})^{1/2}}{(\hat{s}^2/\hat{n}+6)^{1/4}\left(2\hat{s}/\sqrt{\hat{n}}+\sqrt{(\hat{s}^2/\hat{n}+6)}\right)^{1/2}} \tag{2.64}$$

(with opposite sign for Neumann data) and phase

$$-\left(\frac{5}{54}\hat{s}^3+\frac{1}{3}\hat{s}\hat{n}-\frac{2}{27}\left(\hat{s}^2+6\hat{n}\right)^{3/2}\right), \tag{2.65}$$

matching precisely the inner form of the specular field (2.9).

Hence, we have now constructed the full range of solutions (indicated schematically in Figure 2) and have demonstrated smooth matches everywhere and this completes the calculation for the open, convex boundary. We now go on to consider and discuss some of the generalisations to a closed, convex boundary.

3 Scattering by finite bodies

An obvious but crucial difference between infinite and finite scatterers is that the infinite body engenders a well-defined shadow region into which the incident field never propagates and where the solution is exponentially small. The finite case is different, since (i) creeping rays can repeatedly circulate the scatterer, and (ii) at any frequency we can always examine the solution at sufficiently large distances that the body appears point-like and then the incident field dominates almost everywhere. Of course, there is still a smaller underlying diffracted field created by the presence of the scatterer. Because we are considering scattering obstacles with an $O(1)$ aspect ratio, we may take a typical length-scale of the body to be unity without any loss of generality. We also only consider one circulation of the creeping ray around the body; further circulations give rise to exponentially subdominant contributions to the creeping field.

Before proceeding we recall that, for the infinite body case, the results of §2.5 demonstrate that the transition from the illuminated region (where the incident field dominates) to deep shadow (where the creeping field dominates) occurs in a wedge-shaped region with an $O(k^{-\frac{1}{3}})$ included angle, at the outer edges of which the solution takes the form implied by (2.63). Embedded within this is a narrower parabolic region of width $O(k^{-\frac{1}{2}})$ in which the structure is given by (2.53).

For the finite body, we would expect there to be two such wedge-shaped regions, one emanating from each of the two points of tangency with the overall shadow zone occupying the region between them. Clearly these wedges must eventually meet, this being a measure of the onset of the disappearance of the shadow region. The first features to merge are the two "interior" transition zones, by which we mean those bordering deep shadow; this happens at a distance $x = O(k^{\frac{1}{3}})$. Following this, the two complementary error function profiles superpose after distances $x = O(k)$ have been reached. This gradual merging of the shadown boundaries is shown schematically in Figure 3. Region I in this figure, corresponding to x of order one, is covered by the preceding sections. Let us now give a detailed description of the amplitude profile of the total field in the other regions.

Region II: $x = O(k^{1/3})$ We begin by considering the merging of the **transition zones**, the structure of which is given by (2.63) for the single point of ray tangency. Writing $x = k^{1/3}\bar{x}$, with $\bar{x}$ and y of order one, the solution is given simply by the superposition of the transition zone solutions from the "top" and "bottom" boundary points of ray tangency. Labelling these points (x_t, y_t) and (x_b, y_b), respectively, we have

$$\begin{aligned}\phi \quad \sim \quad & k^{-1/3}\bar{x}^{-1/2}e^{ikx}\left(\exp\left(\frac{ik^{2/3}(y-y_t)^2}{2(\bar{x}-k^{-1/3}x_t)}\right) g\left(\frac{(y-y_t)}{\bar{x}};\kappa_t\right)\right. \\ & \left. + \exp\left(\frac{ik^{2/3}(y-y_b)^2}{2(x-k^{-1/3}x_b)}\right) g\left(-\frac{(y-y_b)}{\bar{x}};\kappa_b\right)\right) \qquad (3.1)\end{aligned}$$

plus a plane wave if $y > y_t$ or $y < y_b$. The function g arising in this expression is given by (2.63) ((2.63$'$) in the Appendix for Neumann data). In (3.1), we have made explicit the dependence of g upon the curvature at the point of ray tangency – this is given by κ_t at (x_t, y_t) and κ_b at (x_b, y_b).

The solution (3.1) is valid so long as y is not close to y_t or y_b. For $y - y_t = O(k^{-2/3})$ or $y - y_b = O(k^{-2/3})$, (3.1) matches into the Fresnel integral shadow boundary solutions, which smoothly switch on and off the incident plane wave.

Region III: $x = O(k)$ Let us now consider the region in which these two shadow boundary solutions merge with each other, which occurs for $x = O(k)$. Let us first consider the solution for the transition zones at this distance.

The exponential factors of the form $e^{ik(y-y_t)^2/2(x-x_t)}$ in (3.1) cease to be valid for very large x, with more and more such terms being required as the scaling for x increases. For example, if the scalings are $x = k^nX,\ y = k^{n-1/3}Y$ for large n, then what we find is that the ansatz (2.57) must be modified so that $k^{1/3}\tilde{u}$ is replaced by $k^{(n+1)}\sum_{m=0}^{[3(n+1)/2]} k^{-2m/3}\tilde{u}_m(X,Y)$. Following the calculation through then establishes that the exponent in the corresponding exponential factor combined with that from the factor $e^{ik(x-x_t)}$ reproduces the Taylor series expansion for $\left((x-x_t)^2 + (y-y_t)^2\right)^{1/2}$ under these scalings, and similarly for the lower point of tangency. Hence they can all be encompassed at once by the simple expedient of replacing

$$x^{-1/2}e^{ikx}e^{ik(y-y_t)^2/2(x-x_t)}g\left(\frac{k^{1/3}(y-y_t)}{x};\kappa_t\right)$$

by

$$x^{-1/2}e^{ikx_t}e^{ik((x-x_t)^2+(y-y_t)^2)^{1/2}}g\left(\frac{k^{1/3}(y-y_t)}{x};\kappa_t\right).$$

Thus, with the scalings $x = k\tilde{x}$, $y = k^{2/3}\tilde{y}$, the solution in the transition zone is

$$\phi \sim e^{ikx} + k^{-2/3}\tilde{x}^{-1/2}e^{ik((x-x_\alpha)^2+(y-y_\alpha)^2)^{1/2}}\left(e^{ikx_t}g\left(\frac{\tilde{y}}{\tilde{x}};\kappa_t\right) + e^{ikx_b}g\left(\frac{-\tilde{y}}{\tilde{x}};\kappa_t\right)\right). \qquad (3.2)$$

Note that the incident wave is now present everywhere in this region. This expansion is valid away from $\tilde{y} = 0$. With $\tilde{y} = O(k^{-2/3})$, $y = O(1)$ this solution matches into the field corresponding to the merged complementary error function profiles, which is

$$\phi \sim e^{ikx}\left\{1 + \frac{1}{2}\left[\operatorname{erfc}\left(-\frac{e^{-i\pi/4}(y-y_t)}{\sqrt{(2\tilde{x})}}\right) - \operatorname{erfc}\left(-\frac{e^{-i\pi/4}(y-y_b)}{\sqrt{(2\tilde{x})}}\right)\right]\right\}. \tag{3.3}$$

Region IV: Far field Let us now consider the ultimate far field $r \to \infty$. At these large distances it is appropriate to seek a solution

$$\phi \sim e^{ikx} + e^{ikr}v(r,\theta;k). \tag{3.4}$$

Then, to leading order (in r), v satisfies

$$2\frac{\partial v}{\partial r} + \frac{v}{r} = 0 \tag{3.5}$$

from which

$$v(r,\theta;k) = \frac{G(\theta;k)}{r^{\frac{1}{2}}} \tag{3.6}$$

is immediate. The function G is the diffraction coefficient for the far-field scattered radiation pattern and this is what interests us here, particularly its behaviour in the vicinity of the far-field limit of the shadow region (i.e. for small values of θ). By matching with the asymptotic solutions described thus far, we will determine G in the limit $k \to \infty$.

The far-field for $\theta = O(1)$ can be calculated from (2.9) and is given by

$$\phi_{\text{ref}} \sim -\left[\frac{\sin\frac{1}{2}\theta}{2\kappa(s)r}\right]^{\frac{1}{2}} e^{ikr-ik(x_0(s)\cos\theta + y_0(s)\sin\theta)} \tag{3.7}$$

(with a '+' sign for Neumann data) from which

$$G \sim -\left[\frac{\sin\frac{1}{2}\theta}{2\kappa(s)}\right]^{\frac{1}{2}} e^{-ik(x_0(s)\cos\theta + y_0(s)\sin\theta)}, \tag{3.8}$$

where $(x_0(s), y_0(s))$ is the point of emergence of the reflected ray from the scatterer and the angle of curvature $\psi(s) \sim \theta/2$. When $\theta = O(k^{-1/3})$ we move out of the illuminated region and into the transition zones. Taking the far-field limit of (3.2) with $\theta = k^{-1/3}\hat{\theta}$ gives

$$\begin{aligned} G \quad \sim \quad & k^{-1/6}\left(e^{-ik^{2/3}y_t\hat{\theta} + \frac{1}{2}ik^{1/3}x_t\hat{\theta}^2 + \frac{1}{6}iy_t\hat{\theta}^3} g\left(\hat{\theta};\kappa_t\right)\right. \\ & \left. + e^{-ik^{2/3}y_b\hat{\theta} + \frac{1}{2}ik^{1/3}x_b\hat{\theta}^2 + \frac{1}{6}iy_b\hat{\theta}^3} g\left(-\hat{\theta};\kappa_b\right)\right), \end{aligned} \tag{3.9}$$

to leading order in this region. The outer limit of this expression as $|\hat{\theta}| \to \infty$ must match the inner limit of (3.8). A straightforward calculation shows that if $s = s_\alpha$ is the arclength at the point of tangency ($\alpha = t$ or b), then the appropriate scaling for s in (3.8) is $s = s_\alpha - \dfrac{k^{-1/3}}{2\kappa_\alpha}\hat{\theta}$ and the corresponding inner form is

$$\begin{aligned} G \sim -\tfrac{1}{2}k^{-\frac{1}{6}}\hat{\theta}^{\frac{1}{2}} \quad & \left(e^{-ik^{\frac{2}{3}}y_t\hat{\theta} + \frac{1}{2}ik^{\frac{1}{3}}x_t\hat{\theta}^2 + \frac{1}{6}iy_t\hat{\theta}^3 - \frac{1}{8}i\hat{\theta}^3/\kappa_t}\,\kappa_t^{-\frac{1}{2}}\right. \\ & \left. + e^{-ik^{\frac{2}{3}}y_b\hat{\theta} + \frac{1}{2}ik^{\frac{1}{3}}x_b\hat{\theta}^2 + \frac{1}{6}iy_b\hat{\theta}^3 - \frac{1}{8}i\hat{\theta}^3/\kappa_b}\,\kappa_b^{-\frac{1}{2}}\right). \end{aligned} \tag{3.10}$$

A separate calculation confirms that this is the outer limit of (3.9).

Since the merged shadow boundaries are parabolic, in the far field they correspond to $\theta = O((kr)^{-1/2})$. Thus they affect the directivity on the ray $\theta = 0$ only. Taking the far field of (3.3) gives

$$\phi \sim e^{ikx}\left(1 + \frac{(y_t - y_b)e^{-i\pi/4}}{\sqrt{(2\pi kx)}}\right). \tag{3.11}$$

Hence the directivity for $\theta = 0$ is

$$G \sim \frac{(y_t - y_b)e^{-i\pi/4}}{\sqrt{(2\pi k)}}.$$

This matches into the higher-order corrections to (3.9).

Note that we have found that $G(\theta, k)$ is of order one in k when θ is of order one, of order $k^{-1/6}$ when θ is of order $k^{-1/3}$, and of order $k^{-1/2}$ when $\theta = 0$.

4 Discussion

We have now succeeded in obtaining a leading-order asymptotic description, covering all regions of space, for the total wavefield engendered as a result of an incoming ray impinging upon a scattering obstacle along a tangent. We have also gone on to use these results to discuss scattering by finite obstacles and, in both cases, have presented the analyses systematically using matched asymptotic expansions.

In the latter case, we found that the ultimate far-field merging of the transition zones bordering each shadow boundary leads to a delicate structure in the scattered field; more precisely, a highly collimated wave structure (given by (3.9)) persists for arbitrarily large distances and is the only remnants of the complicated shadow zone structure apparent at lesser distances. The 'directivity' that is valid here carries as parameters the curvatures of the boundary at the two points of ray tangency and it might well be the case that careful measurement of the wavefield in this region could lead to a way of determining these curvatures experimentally in a given practical situation. This has implications for the inverse problem of determining the geometry of a scatterer, which might be an inclusion or void in an electromagnetic, acoustic or elastic medium, by such a measurement; if the incident field is generated by a sufficiently remote transducer, for example, then by simply changing the relative angular direction between the transducer and scatterer and repeating the measurement each time, it should be possible to generate a profile of the obstruction. Ideas on such reconstructions in this high-frequency limit are given by Kriegsmann [19]

We have seen that the creeping field that is initiated at points of ray tangency and has an exponentially decaying amplitude of roughly $O(e^{-ck^{\frac{1}{3}}s})$, where c is a constant that can be read off from (2.36) and s is the arclength traversed by the surface ray. This is in sharp contrast to creeping wave propagation on a slender body of $O(k^{-\frac{1}{2}})$ aspect ratio for which creeping field amplitude profiles have an *algebraic* dependence upon k [13]. Despite the exponential decay rate in this case we remark that high-frequency approximations in wave theory – particularly those based around ray methods, as here – have a tendency to be valid and to give remarkably accurate results for much smaller values of the large parameter (k, in this case) than might be expected. Though not relevant to the case we have considered, a good example is the analysis of diffraction by an aperture [20] where in certain cases plots of the asymptotic results agree well with those of the exact solution for values of the normalised controlling asymptotic parameter (k, essentially) as small as one or two.

Practical implementations of the results we present here might use such 'intermediate' values of k, in which case the creeping fields and the associated diffracted radiation may well become measurable effects beneath the larger reflected field. Of course, their 'inner' structure near their points of initiation is a crucial feature of the local wavefield that feeds into the $O(k^{-\frac{1}{6}})$ far-field "shadow" pattern discussed in §3.

Extensions of this work to include more general incident wavefields is possible. If the incoming wave is generated by a remote (i.e. at order-one distance) line-source then the wavefronts near the points of tangency are locally planar and the Fock-Leontovič analysis presented in Section 2.2 carries over with minor modifications; however, we remark that whilst the shadow boundary structure corresponding to each of the two tangent rays can be deduced from the results of Section 2.5, the 'merging' phenomena are different in this case and do not necessarily follow from Section 3. This is because the geometrical shadow boundaries (i.e. the continuation of the tangent rays) diverge in this configuration whereas they are parallel for the plane wave case discussed in this paper. For very remote sources, the canonical cases are

(i) a source at a distance of order $k^{1/3}$, in which case the divergence of the geometrical shadow boundaries affects the primary merging of the transition zones, the Fresnel regions never merge, and the shadow persists for arbitrarily large distances in that the incident field is absent from the wedge-shaped geometrical shadow, and

(ii) a source at a distance of order k, in which case the primary merging of the transition zones is unaffected but the divergence of the geometrical shadow boundaries affects the merging of the Fresnel regions. This is the limiting case for the disappearence of the shadow at large distances. The far-field directivity is the same as that for a plane wave except on the line $\theta = 0$.

Gaussian beam incidence can be analysed using the prescription for beam generation by locating a line source at a complex point due to Deschamps [21]. In this case, care must be taken to analyse the complex ray structure of the scattered field in terms of certain Stokes surfaces responsible for 'switching-on' and 'switching off' complex ray fields in certain regions of the physical domain. A recipe for doing this is presented in [22], in which a preliminary discussion of tangential diffraction of an *inhomogeneous* plane wave is discussed.

Other natural extensions are a treatment of the vector case – as is appropriate for some situations in electromagnetic and elastic wave scattering (though we remark that a good number of these cases can be reduced to the scalar problems considered here) – and three-dimensional problems, the latter being considered by Saward [23], who analyses diffraction by bodies of revolution (and radiation from boundary sources in more general three-dimensional geometries) in much the same spirit to that used here.

Acknowledgements

BJS and IZ are grateful for the provision of mathematics studentships by EPSRC and the Government of Pakistan, respectively. SJC is supported by a Royal Society University Research Fellowship. RHT, SJC and JRO gratefully acknowledge the support of the Smith Institute, Guildford, where many discussions related to this work took place. Finally, we are indebted to Drs Colin Sillence and Jill Ogilvy of British Aerospace for their continued interest in this work.

Appendix

The results presented in the main body of the paper are for Dirichlet boundary data; where there is a difference for Neumann data we have listed the analogous results below adopting the convention that the 'Neumann equivalent' of equation (2.9), for example, is given in this Appendix in equation (2.9′). Where no alternative equations are listed here, it can be taken that the result being discussed in the text is valid for both boundary conditions, unless stated explicitly otherwise.

$$\frac{\partial \phi}{\partial n} = 0 \quad \text{on} \quad \partial D \tag{2.3′}$$

$$\phi_r \sim \left[\frac{\sin\psi(s)}{2\kappa(s)\tau + \sin\psi(s)}\right]^{\frac{1}{2}} e^{ik(x_0(s)+\tau)} \tag{2.9′}$$

$$\frac{\partial \hat{A}}{\partial \hat{n}}(\hat{s},0) = -i\hat{s}e^{-i\hat{s}^3/6} \tag{2.13′}$$

$$\hat{A}(\hat{s},\hat{n}) = -2^{\frac{1}{3}}e^{-2\pi i/3}\int\limits_{-\infty}^{\infty}\frac{\mathrm{Ai}'(-2^{\frac{1}{3}}p)\mathrm{Ai}\left(-2^{\frac{1}{3}}(p+\hat{n})e^{2\pi i/3}\right)e^{-i\hat{s}p}}{\mathrm{Ai}'\left(-2^{\frac{1}{3}}pe^{2\pi i/3}\right)}dp \tag{2.15′}$$

$$\frac{\partial \hat{B}}{\partial \hat{y}} + i\hat{x}\hat{B} = -i\hat{x}, \quad \hat{y} + \tfrac{1}{2}\hat{x}^2 = 0 \tag{2.19′}$$

$$\frac{\partial \hat{\omega}}{\partial \hat{\xi}} = -i\hat{\xi}e^{-i\hat{\xi}^3/6}, \quad \hat{\xi} = 0 \tag{2.23′}$$

$$f'(s) = -\frac{\mu_m^2\kappa^{\frac{2}{3}}(s)e^{-2\pi i/3}}{2^{\frac{1}{3}}}, \quad \mathrm{Ai}'(-\mu_m^2) = 0 \quad \text{with} \quad (\mu_0 < \mu_1 < \mu_2 \ldots). \tag{2.29′}$$

$$A_R(\hat{s},\hat{n}) = -2\pi i e^{-\pi i/3}\sum_{m=0}^{\infty}\frac{\mathrm{Ai}'\left(-\mu_m^2e^{-2\pi i/3}\right)\mathrm{Ai}(-\mu_m^2 - 2^{\frac{1}{3}}e^{2\pi i/3}\hat{n})\exp(-i2^{-\frac{1}{3}}e^{-2\pi i/3}\mu_m^2\hat{s})}{\mu_m^2\mathrm{Ai}(-\mu_m^2)} \tag{2.37′}$$

$$\alpha_0 = \frac{-2\pi i e^{-i\pi/3}\mathrm{Ai}'\left(-\mu_0^2e^{-2\pi i/3}\right)}{\mu_0^2\mathrm{Ai}(-\mu_0^2)\kappa_0^{1/6}}, \quad \beta_0 = 0 \tag{2.38′}$$

$$F_0(\rho) = -\frac{\pi^{\frac{1}{2}}e^{i\pi/4}2^{1/6}\mathrm{Ai}'\left(-\mu_0^2e^{-2\pi i/3}\right)}{\kappa_0^{1/6}\kappa^{1/6}(\rho)\mu_0^2\mathrm{Ai}(-\mu_0^2)} \tag{2.47′}$$

$$v(\rho) = -\mu_0^2e^{-2\pi i/3}2^{-\frac{1}{3}}\int_0^{\rho}\kappa^{2/3}(t)dt \tag{2.48′}$$

$$g(\xi) = -(2\pi)^{-1/2}\kappa_0^{-1/3}e^{-7\pi i/12}e^{-i\xi^3/6\kappa_0}\int\limits_{-\infty}^{\infty}\frac{\mathrm{Ai}'(-2^{1/3}p)}{\mathrm{Ai}'(-2^{1/3}pe^{2\pi i/3})}e^{ip\xi/\kappa_0^{1/3}}dp \tag{2.63′}$$

References

[1] V.A. Fock, *Electromagnetic diffraction and propagation problems*, New York, Macmillan (1960).

[2] M. Leontovič and V. Fock, "Solution of the problem of propagation of electromagnetic waves along the earth's surface by the method of the parabolic equation", *Jnl. of Physics X*, 13-24 (1945).

[3] J.B. Keller, "Diffraction by a convex cylinder", *URSI Michigan Electromagnetic Wave Theory Symposium*, 312-321 (1955).

[4] J.B. Keller, "Geometrical theory of diffraction", *J. Opt. Soc. Amer. A52*, 116-130 (1962).

[5] J.B. Keller and R.M. Lewis, "Asymptotic methods for partial differential equations: the reduced wave equation and Maxwell's equations', in *Surveys in Applied Mathematics 1* (ed. J.B. Keller, D.W. McLaughlin and G.C. Papanicolaou), 1-82, Plenum Press, New York (1995).

[6] B.R. Levy and J.B. Keller, "Diffraction by a smooth object", *Comm. Pure Appl. Math. XII*, 159-209 (1959).

[7] R.M. Lewis, N. Bleistein and D. Ludwig, "Uniform asymptotic theory of creeping waves", *Comm. Pure Appl. Math. XX*, 295-328 (1967).

[8] E. Zauderer, "Wave propagation around a convex cylinder", *J. Math. Mech. 13*, 171-186 (1964).

[9] E. Zauderer, "Wave propagation around a smooth object", *J. Math. Mech. 13*, 187-199 (1964).

[10] D. Bouche, F. Molinet and R. Mittra, *Asymptotic methods in electromagnetics*, Springer-Verlag, Berlin (1994).

[11] V.M. Babič and V.S. Buldyrev, *Short-wavelength diffraction theory – asymptotic methods*, Springer-Verlag, Berlin (1991).

[12] V.M. Babič and N.Y. Kirpičnikova, *The boundary-layer method in diffraction problems*, Springer-Verlag, Berlin (1979).

[13] J.C. Engineer, J.R. King and R.H. Tew, "Diffraction by slender bodies", *Euro. Jnl. of Applied Mathematics 9*, 129-158 (1998).

[14] D.S. Jones, *Acoustic and electromagnetic waves*, Oxford University Press (1986).

[15] H.M. Nussenzveig, "High-frequency scattering by an impenetrable sphere", *Annals of Physics 34*, 23-95 (1965).

[16] P.H. Pathak, "An asymptotic analysis of the scattering of plane waves by a smooth convex cylinder". *Radio Science 14*, 419-435 (1979)

[17] A. B. Olde Daalhuis, S. J. Chapman, J. R. King, J. R. Ockendon and R. H. Tew, "Stokes phenomenon and matched asymptotic expansions", *SIAM J. Appl. Math.* **55**, 1469-1483 (1995).

[18] R.N. Buchal and J.B. Keller, "Boundary layer problems in diffraction theory", *Comm. Pure Appl. Math. XIII*, 85-114 (1960).

[19] G.A. Kriegsmann, "Acoustic target reconstruction using geometrical optics phase information", *IMA J. Appl. Math. 48*, 243-247 (1992).

[20] J.B. Keller, "Diffraction by an aperture", *J. Appl. Phys. 28*, 426-444 (1957).

[21] G.A. Deschamps, "Gaussian beam as a bundle of complex rays", *Elect. Lett. 7*, 684-685 (1971).

[22] S.J. Chapman, J.M.H. Lawry, J.R. Ockendon and R.H. Tew, "On the theory of complex rays", *Surveys in Applied Mathematics (J.B. Keller, D.W. McLaughlin and G.C. Papanicolaou, Eds.)*, to appear.

[23] V.H. Saward," Some problems in diffraction theory", *D.Phil. Thesis*, University of Oxford (1997).

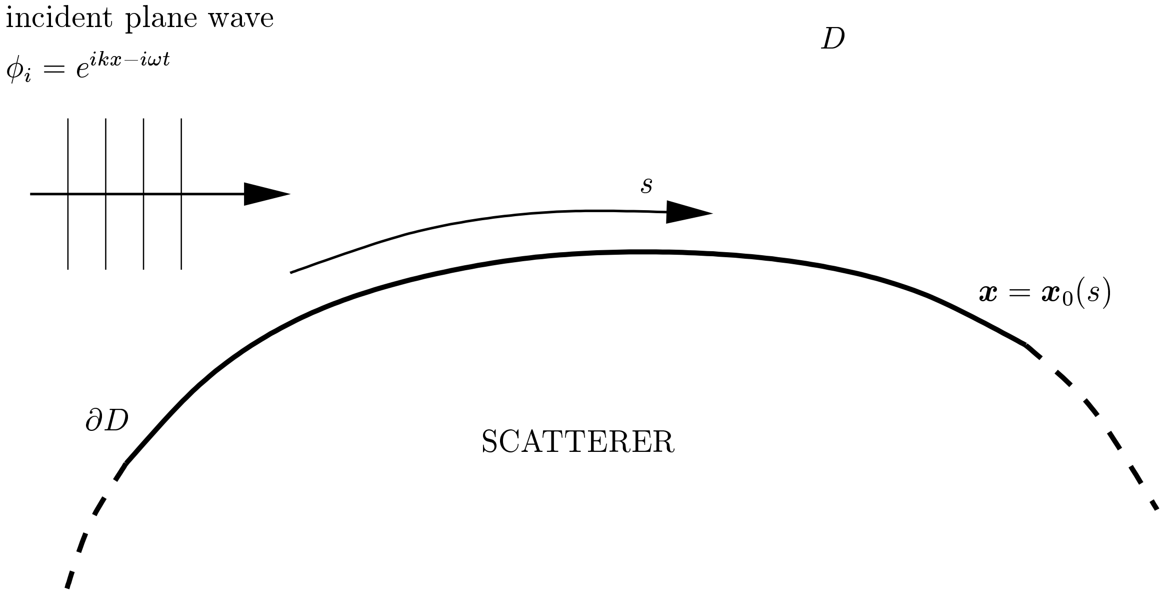

Figure 1: The scattering geometry for an infinite body. Arclength s is measured in a clockwise direction from the point of tangency between the incoming tangent ray and ∂D, which is also taken as the origin for a cartesian coordinate system. The boundary ∂D is convex in D and is open, so that $-\infty < s < \infty$.

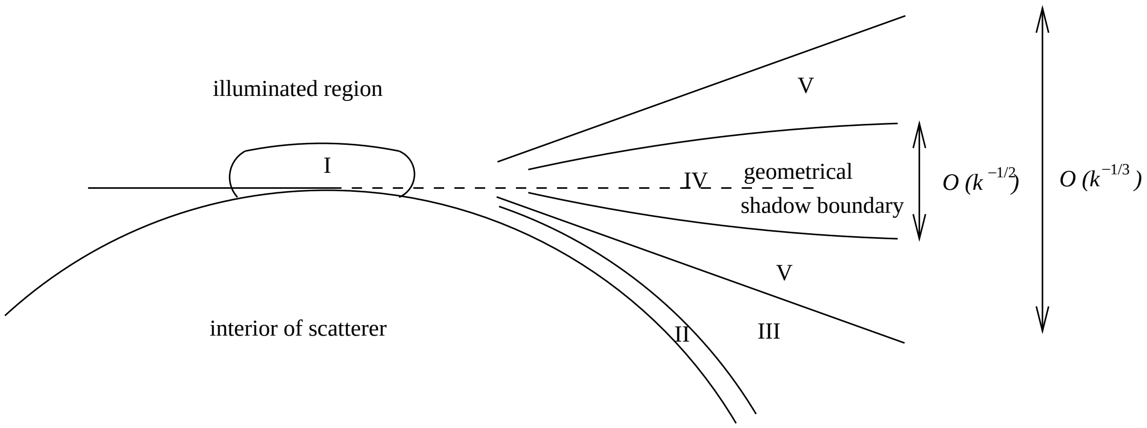

Figure 2: A schematic of the field in the ray tangency and shadow boundary regions. The wave structure in regions I – V is described in the following sections: I (the Fock-Leontovič region) – §2.2; II (the near-surface Airy layer) – §2.3; III (the shadow region) – §2.4; IV (the Fresnel region) – §2.5 (eq$^{\mathrm{n}}$ (2.54)); V (the transition zones) – §2.5 (eq$^{\mathrm{n}}$ (2.63)).

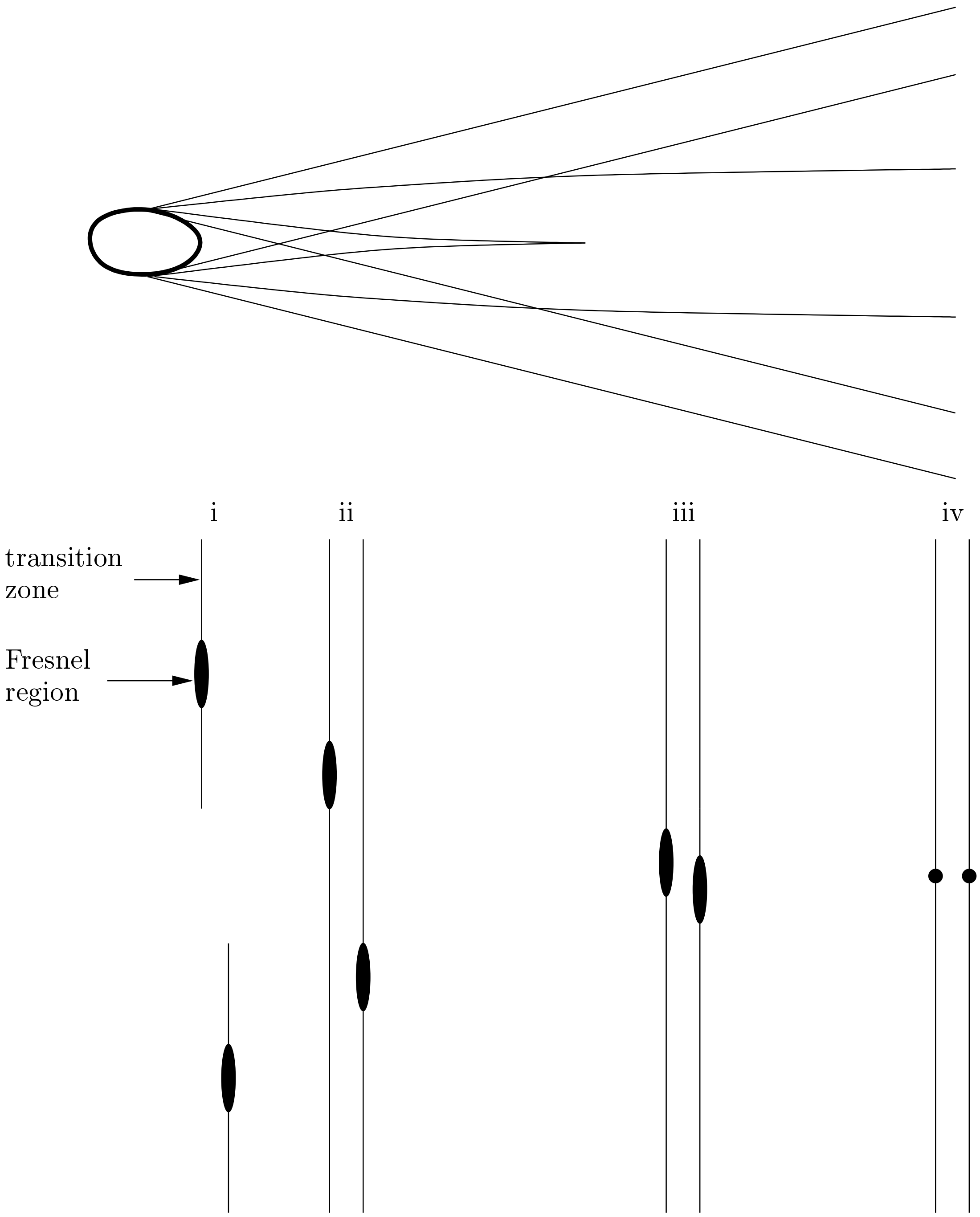

Figure 3: The merging shadow boundaries. The lower half of the figure shows schematically the structure of a slice across the shadow at different values of x. The left-hand lines represent contributions originating at the upper tangency point, while the right-hand lines represent contributions originating at the lower tangency point. (i) $x = O(1)$; distinct Fresnel and transition regions separated by a shadow region. (ii) $x = O(k^{1/3})$; the transition zones merge, but the Fresnel regions are still distinct. (iii) $x = O(k)$; the Fresnel regions merge. (iv) The far field; the Fresnel regions shrink as $r \to \infty$, but the transition zones still affect the directivity for small $(O(k^{-1/3}))$ angles.